SCIENTIFIC REPORTS

OPEN

SUBJECT AREAS:
SURFACES, INTERFACES AND THIN FILMS
STRUCTURAL PROPERTIES

Received
19 March 2014

Accepted
14 July 2014

Published
1 August 2014

Correspondence and requests for materials should be addressed to C.L. (chenglu@uow.edu.au)

Atomistic Simulation of Tensile Deformation Behavior of $\sum 5$ Tilt Grain Boundaries in Copper Bicrystal

Liang Zhang, Cheng Lu & Kiet Tieu

School of Mechanical, Materials and Mechatronic Engineering, University of Wollongong, Wollongong, NSW 2522, Australia.

Experiments on polycrystalline metallic samples have indicated that Grain boundary (GB) structure can affect many material properties related to fracture and plasticity. In this study, atomistic simulations are employed to investigate the structures and mechanical behavior of both symmetric and asymmetric $\sum 5$[0 0 1] tilt GBs of copper bicrystal. First, the equilibrium GB structures are generated by molecular statics simulation at 0K. The results show that the $\sum 5$ asymmetric GBs with different inclination angles (ϕ) are composed of only two structural units corresponding to the two $\sum 5$ symmetric GBs. Molecular dynamics simulations are then conducted to investigate the mechanical response and the underlying deformation mechanisms of bicrystal models with different $\sum 5$ GBs under tension. Tensile deformation is applied under both 'free' and 'constrained' boundary conditions. Simulation results revealed different mechanical properties of the symmetric and asymmetric GBs and indicated that stress state can play an important role in the deformation mechanisms of nanocrystalline materials.

It has long been recognized that grain boundaries (GBs) are important microstructure features and can significantly affect the properties of polycrystalline materials[1]. When the grain size is reduced to ultrafine or nano scale, the effects of GBs on the material properties become more significant since the traditional deformation mechanisms based on nucleation and propogation of lattice dislocation are replaced gradually by GB mediated processes, such as GB sliding[2], grain rotation[3,4], diffusional creep[5], dislocation nucleation or absorption at GB etc.[6–10]. Much experimental work and many atomistic simulations have been conducted to examine various GBs on their energy, structure and properties. However, previous research work has focused primarily on symmetric GBs which possess mirror symmetry of crystallographic planes. In contrast, very few atomistic simulations have been conducted on the structure and related properties of asymmetric GBs, even though experimental observation has shown that most GBs in real polycrystalline materials are actually asymmetric[11–13] and they can affect the material properties more significantly[14,15].

Recently, both experimental observations[16–21] and atomistic simulations[22–27] have been attempted of asymmetric tilt GBs, and these give us a better understanding of the structures and energy on these boundaries and provide insight into the related GB properties, e.g., the structural transformations, dissociations, faceting transitions etc. Much of these works concentrate on the $\sum 3$ family because the most common $\sum 3$ GB is the coherent twin boundary with very low boundary energy and they are more frequently observed in polycrystals[12,13,28–30]. Tschopp and McDowell[26] took advantage of atomistic simulation on both symmetric and asymmetric $\sum 3 < 1\,1\,0 >$ tilt GBs and found that the structure and energy of the asymmetric GBs were closely related to the corresponding symmetric ones. Their investigation[27] on dislocation nucleation from different $\sum 3$ asymmetric boundaries under uniaxial tension demonstrated that the properties of GB depend not only upon the misorientation between grains, but also upon the inclination of the GB plane. Lin[22] and Luo[23] performed simulations on the asymmetric $\sum 3 < 1\,1\,0 > (1\,1\,0)/(1\,1\,4)$ GB in copper bicrystals under shock loading to examine the influence of GB on the mechanical behavior of the bicrystal system. Compared with the productive research findings on $\sum 3$ asymmetric boundaries, very few experiments or simulations have focused on other low index coincident site lattice (CSL) systems. Recently, Tschopp and coworkers[31] investigated the structure and energy of several low CSL bicrystal systems, i.e. $\sum 5$, $\sum 13$ GBs around [0 0 1] misorientation axis and $\sum 9$, $\sum 11$ GBs around [1 1 0] misorientation axis. However, they did not study the correlation between the asymmetric GB structures and their mechanical behavior. H. Zhang performed a series of simulations to examine the influence of GB inclination on the mobility[25], diffusivity[32] and migration[24,33] of $\sum 5$ tilt asymmetric GBs, but no further research was conducted to analyze the mechanical response in relation to the deformation mechanisms at atomic scale.

In this study we carried out molecular dynamics (MD) simulations on two symmetric and four asymmetric $\sum 5$ GBs of copper under tensile deformation to probe their mechanical behavior and the related deformation mechanisms at atomic scale. Although the primary aim of this work is to show the effect of GB inclination on tensile response, the influence of transverse stress on the mechanical behavior is also examined. In the simulations, the tensile deformation is conducted under both 'free' and 'constrained' tension boundary condition, which will be specified in the *methods* section.

Results

GB structure and energy. GB structures are identified using the common neighbor analysis (CNA) technique suggested by Schiøtz et al.[34]. Fig. 1 shows the equilibrium structures of the two symmetric and four asymmetric $\sum 5$ GBs of Cu at 0K which were investigated. The black and white balls correspond to the two adjacent atom layers along the [0 0 1] tilt axis. Structure units as defined by Rittner[35] are used to illustrate the boundary structures. The six-member kite-shaped unit is referred to as the "E" unit which organizes the symmetric $\sum 5$ (3 1 0) ($\phi = 0^\circ$) boundary as outlined in Fig. 1 (a). The symmetric $\sum 5$ (2 1 0) ($\phi = 45^\circ$) is composed of the topologically identical structure unit "E′", which differs only in direction and arrangement along the boundary plane, as shown in Fig. 1 (f). Careful investigation of the four asymmetric GBs shows that all of them are organized by the combination of E and E′ units that correspond to their symmetric $\sum 5$ (3 1 0) and $\sum 5$ (2 1 0) boundaries but with different ratios. In other words, the asymmetric GBs can be decomposed into their corresponding symmetric boundaries. For example, the period vector for the asymmetric $\sum 5$ (9 2 0)/(6 7 0) ($\phi = 30.96^\circ$) is a_0 [7 −6 0] or a_0 [2 −9 0] and this can be separated into one period of the $\sum 5$ (3 1 0) ($\phi = 0^\circ$) symmetric GB and three period of the $\sum 5$ (2 1 0) ($\phi = 45^\circ$) symmetric GBs. This reaction can be described by:

$$a_0[7\ -6\ 0] = a_0[1\ -3\ 0] + 3a_0[2\ -1\ 0] \quad (1)$$

$$\text{or } a_0[2\ -9\ 0] = a_0[-1\ -3\ 0] + 3a_0[1\ -2\ 0] \quad (2)$$

It should be noted that the ratio of E unit to E′ unit decreases with the increase of inclination angle ϕ and the equal ratio is found in the $\sum 5$ (1 0 0)/(4 3 0) ($\phi = 18.43^\circ$) boundary, as shown in Fig. 1 (c). This finding that asymmetric GBs can facet into their corresponding symmetric ones is similar to the finding of the $\sum 3$[1 1 0] grain boundary family[26].

Since the structures of asymmetric GBs are closely related to their corresponding symmetric boundary structures, a faceting model is proposed to predict the energy of asymmetric GBs with idea faceting structures, i.e. the energy of the faceted asymmetric boundaries can be predicted by simply using a weighted fraction of the relative contribution of facet lengths times the respective symmetric boundary energy[31]. This relationship can be expressed by the following equation,

$$\gamma_A = \gamma_{S1} \cdot \left[\cos\Phi - \sin\Phi\left(\frac{\cos\alpha}{\sin\alpha}\right)\right] + \gamma_{S2}\left[\frac{\sin\Phi}{\sin\alpha}\right] \quad (3)$$

where γ_A is the predicted energy of the asymmetric GB with different inclination angles ϕ, γ_{S1} and γ_{S2} are the calculated energy of the two corresponding symmetric GBs, α is the interval angle separating the two symmetric GBs which depends on the crystal symmetry around

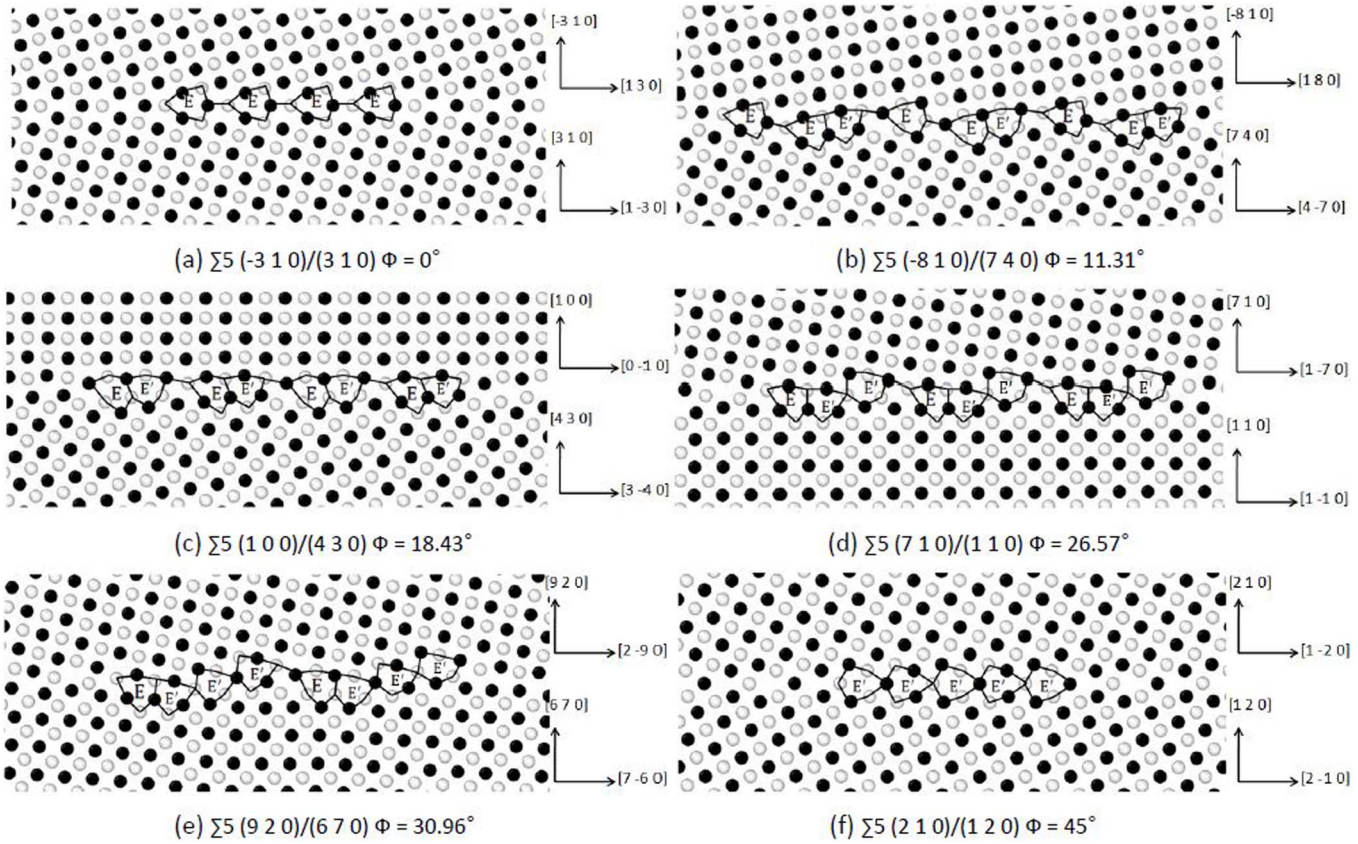

Figure 1 | $\sum 5$ GB structures of Cu for various inclination angles ϕ at 0K. The structures are viewed along the [0 0 1] tilt axis, atoms on consecutive (0 0 2) plane are shown as black and white. The boundary normal vector of grain A and grain B are marked on the right-hand side for each GB. The structure unit at each boundary plane are outlined by the solid line as marked by E and E′. (a) and (f) are the two symmetric GBs, (b)–(e) are the four asymmetric GBs.

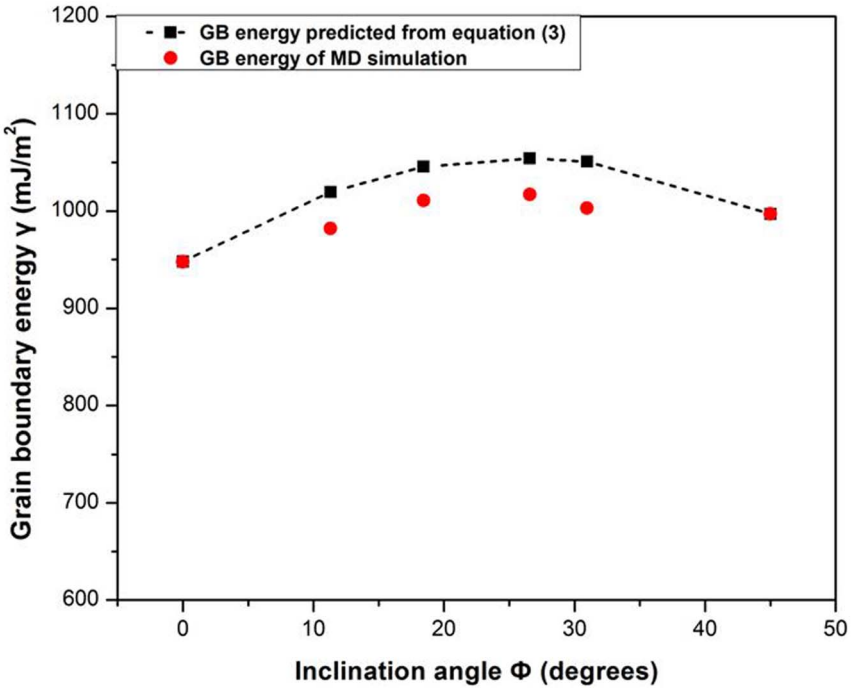

Figure 2 | Grain boundary energy as a function of inclination angle of six ∑5 GBs. The solid square is the predict GB energy from equation (3), the dotted line is fitted by the predicted results which represents the trend of energy for ∑5 asymmetric GBs. The solid dot is the GB energy of MD simulation.

the tilt axis ($\alpha = 30^\circ$ for [1 1 1] axis, $\alpha = 45^\circ$ for [0 0 1] axis and $\alpha = 90^\circ$ for [1 1 0] axis). Here, the calculated energy of the two ∑5 symmetric GBs is 948 mJ/m^2 and 997 mJ/m^2 respectively, the predicted energy value according to equation (3) and the calculated energy value from MD simulation of the four asymmetric GBs are plotted in Fig. 2. The consistent trend and small deviation between the predicted and the calculated energy values indicates that the faceting of asymmetric GBs into the structure units of the corresponding symmetric GBs is favorable from the point of view of energy.

Mechanical response and deformation mechanism. Tensile simulations are conducted under free tension boundary condition and constrained tension boundary condition respectively, the simulation is specified in the *method* section. Fig. 3 (a) and (b) show the tensile stress-strain response of bicrystal models with different ∑5 GBs at 10 K. For the mechanical properties, the system stress is attained by calculating the pressure of the entire system of atoms, system strain is derived from the positions of the periodic boundaries. On the whole, the maximum tensile stress of the two symmetric GBs ($\phi = 0^\circ$ and $\phi = 45^\circ$) is higher than the peak stress of the four asymmetric GBs. The mechanical behavior of different ∑5 GBs can be associated with their energy, as seen in Fig. 2. As calculated in the simulation, ∑5 ($\phi = 0^\circ$ and $\phi = 45^\circ$) GB shows the comparative lower energy, so it may have the more stable structure and the tensile strength is higher. It is worth noting that the maximum tensile stress of each case under constrained boundary condition is significantly higher than the value of free boundary condition. The higher tensile stress can be attributed to the stress that developed transverse to the loading direction during the deformation process.

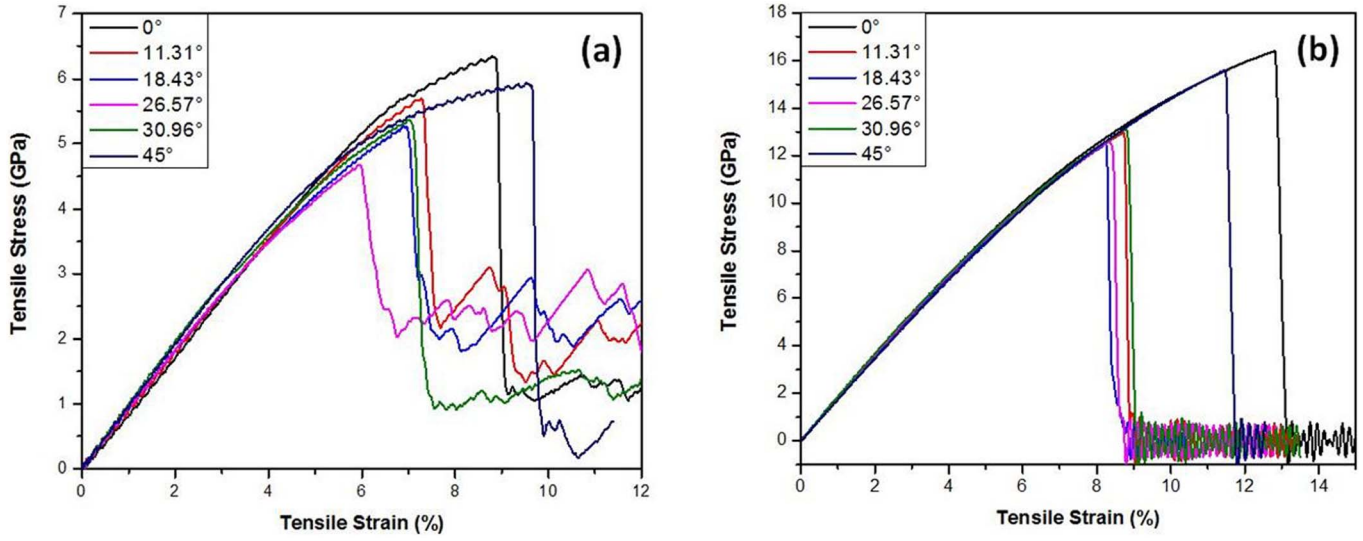

Figure 3 | Mechanical response of ∑5 GBs with different inclination angles ϕ at 10 K under (a) free tension boundary condition and (b) constrained tension boundary condition.

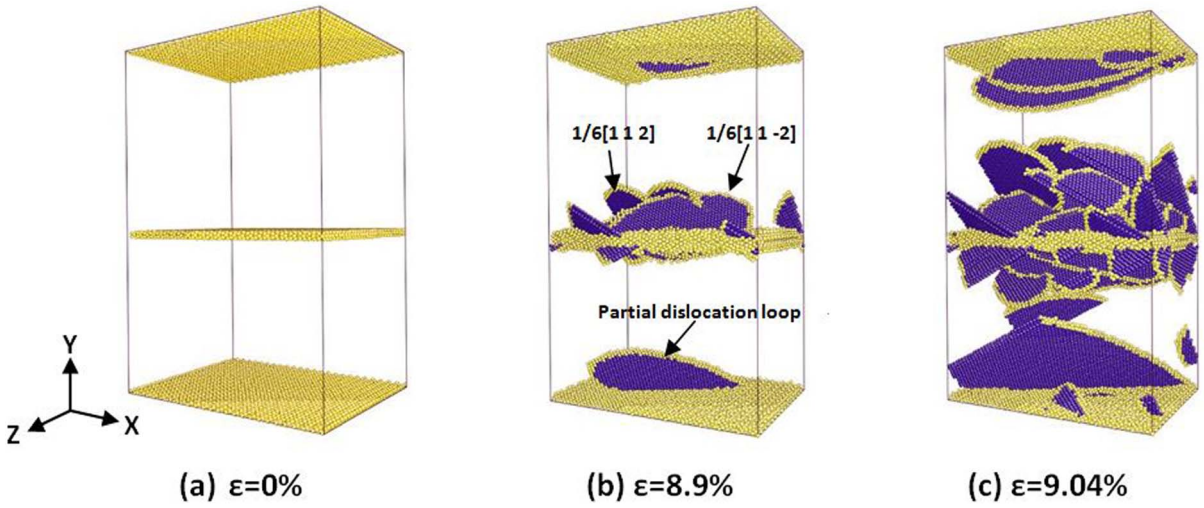

Figure 4 | Snapshots of Cu bicrystal with $\sum 5$ ($\phi = 0^\circ$) GB at different deformation stage under free tension boundary condition. Images are colored according to the CNA parameter. Atoms with perfect fcc structures are removed to facilitate viewing of the defective structures. Atoms colored with yellow organize the GB plane and the dislocation core, while the blue atoms represent the stacking fault.

Visual inspection of the MD simulation results indicates that the maximum tensile stress corresponds to the nucleation of partial dislocations, in agreement with results for uniaxial tensile of Cu bicrystal by Spearot et al.[27,36]. Fig. 4 shows the snapshot of atoms in Cu bicrystal with $\sum 5$ ($\phi = 0^\circ$) GB at different deformation stages under free tension boundary *condition*. Images are colored according to the CNA parameter. Atoms with perfect fcc structures are removed to facilitate viewing of the defective structures. Atoms colored with yellow organize the GB plane and the dislocation core, while the blue atoms represent the stacking fault. The dislocation extraction algorithm (DXA)[37,38] is used to compute their Burgers vectors. The GB region becomes coarsening when the tensile deformation is increasing until the maximum tensile stress has been reached. In Fig. 4 (b), at the beginning of the stress drop ($\varepsilon = 8.9\%$), the image shows that partial dislocation loops with both edge and screw character are nucleated from the bicrystal interface into the upper grain and the lower grain simultaneously. DXA analysis indicates that Shockley partial dislocation with Burger's vectors $\mathbf{b} = (1/6)[1\ 1\ 2]$ and $\mathbf{b} = (1/6)[1\ 1\ -2]$ nucleated from the bicrystal interface and slip on the (1 1 1) and (1 1 −1) plane. According to the Schmid factor analysis, they are the most favorable slip system. The tensile stress required to nucleate the first partial dislocation from the $\sum 5$ ($\phi = 0^\circ$) GB at 10 K is calculated as 6.28 GPa, which corresponds to a critical resolved shear stress of approximately 3.08 GPa for the given lattice orientation. The result is comparable to the maximum resolved shear stress under the uniaxial tensile deformation of bicrystal Cu at 300 K by Spearot[39]. With the increase in the tensile strain, dislocations nucleate continuously from the GB plane and slip in each grain, as seen in Fig. 4 (c).

Fig. 5 shows the atomic details of Cu bicrystal with $\sum 5$ ($\phi = 11.31^\circ$) GB at different deformation stages under free boundary condition. Atoms are colored by the CNA parameter and remove the atoms with fcc structures to facilitate the defective structures. The GB region expands and becomes coarsened when deformation occurs. Then, partial dislocations with Burger's vectors $\mathbf{b} = (1/6)[1\ 1\ 2]$ and $\mathbf{b} = (1/6)[1\ 1\ -2]$ are nucleated in the lower grain region, as shown in Fig. 5 (b) at $\varepsilon = 7.3\%$. However, unlike the case of $\sum 5$ ($\phi = 0^\circ$) GB, dislocation nucleates into only one crystal lattice when the maximum tensile stress has been reached. This phenomenon can be attributed to the asymmetric GB with different orientation angles in the two lattices. Partial dislocations are nucleated and emitted continuously into the lower grain until the tensile strain reaches $\varepsilon = 7.6\%$, as shown in Fig. 5 (c). The slip system is now activated in the upper grain, evidenced by a partial dislocation with Burger's vectors $\mathbf{b} = (1/6)[1\ 1\ 2]$ nucleated from the interface and slip along the (1 1 −1) plane. After that, dislocation slips collectively in both grain regions

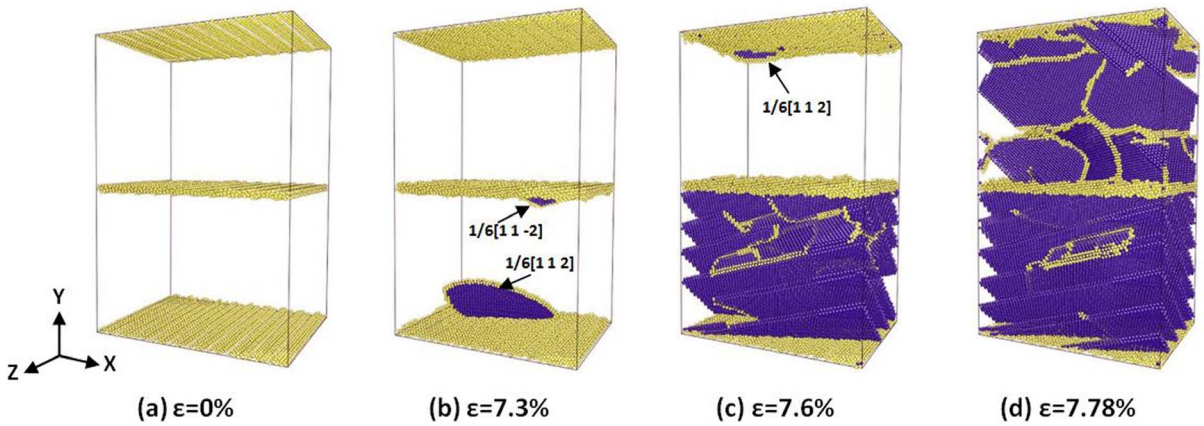

Figure 5 | Snapshots of Cu bicrystal with $\sum 5$ ($\phi = 11.31^\circ$) GB at different deformation stage under free tension boundary condition. Images are colored according to the CNA parameter. Atoms with perfect fcc structures are removed to facilitate viewing of the defective structures. Atoms colored with yellow organize the GB plane and the dislocation core, while the blue atoms represent the stacking fault.

accommodate the plastic deformation during the tensile process. The same phenomena has been observed in other cases of Cu bicrystals with asymmetric GB, as shown in S-Fig. 2

Fig. 6 shows the different deformation stages of Cu bicrystal with $\sum 5$ ($\phi = 18.43^{\circ}$) GB when subjecting to tensile deformation under constrained boundary condition. Fig. 6 (a)–(c) gives the projected view of the atomic snapshots, atoms with perfect fcc structure are rendered as dark blue, atoms at GB area and the dislocation core are rendered as yellow, the light blue atoms indicate the stacking fault. Dislocations are extracted and they are converted to continuous lines, as shown in Fig. 6 (d)–(f). In the elastic deformation stage, all the boundary atoms are well organized and the GB keeps its equilibrium configuration until the maximum tensile stress is achieved. Fig. 6 (a) corresponds to the initial stage of the plastic deformation when a crack is initiated on 'grain boundary 1' and 'grain boundary 2' simultaneously (as introduced in *Methods* section, the periodic boundary condition applied in the Y direction introduces a second boundary plane). Atoms are beginning to shuffle at the crack tips where partial dislocation has nucleated, as seen in the enlarged area in Fig. 6 (a). Again, DXA analysis indicates the slip of partial dislocations occurring on both activated (1 1 1) and (1 1 −1) planes in the lower grain region, which is in agreement with Schmid factor analysis. As the tensile strain increases, the fast decline of tensile stress is associated with the progressive separation of the GBs as well as the partial dislocation nucleation from the crack tips, as seen in Fig. 6 (b) and (e). The high density of the dislocation network at $\varepsilon = 8.44\%$ only stays for a short period and soon decreases gradually with the cleavage of the GB plane and the separation of the two grains, as seen in Fig. 6 (c) and (f). Interestingly, the dislocation is not seen to be emitted into the upper grain region during the tension process. Unlike the massive dislocations and their slipping in the bicrystal models under free tension boundary condition, only limited dislocations are observed in the cases studied under constrained boundary condition. The crack initiates and extends along the GB plane in a cleavage manner and eventually results in the fracture of the model, as shown in S-Fig. 3.

Discussion

Different from the symmetrical GBs which possess mirror symmetry of crystallographic planes, asymmetric GBs are relative complex with a multiplicity of atomic structures resulting from the boundary dissociation, nano-faceting, and other fundamentally interesting structural effects. Simulations[26,31] revealed that asymmetric GBs tend to break into nano-scale facets which are composed of their corresponding symmetric boundaries. Sutton and Balluffi[40] proved that the faceting of an asymmetric GB into a symmetric GB is a geometrical possibility. This is also confirmed in our simulation of the $\sum 5$ GBs where all the asymmetric boundaries are organized by the combination but different ratio of E and E′ structure units which correspond to the $\phi = 0^{\circ}$ and $\phi = 45^{\circ}$ symmetric boundary respectively. However, a recent study of $\sum 11$ [1 1 0] tilt GBs[41] with different inclination angles revealed that it is not necessary for the asymmetric

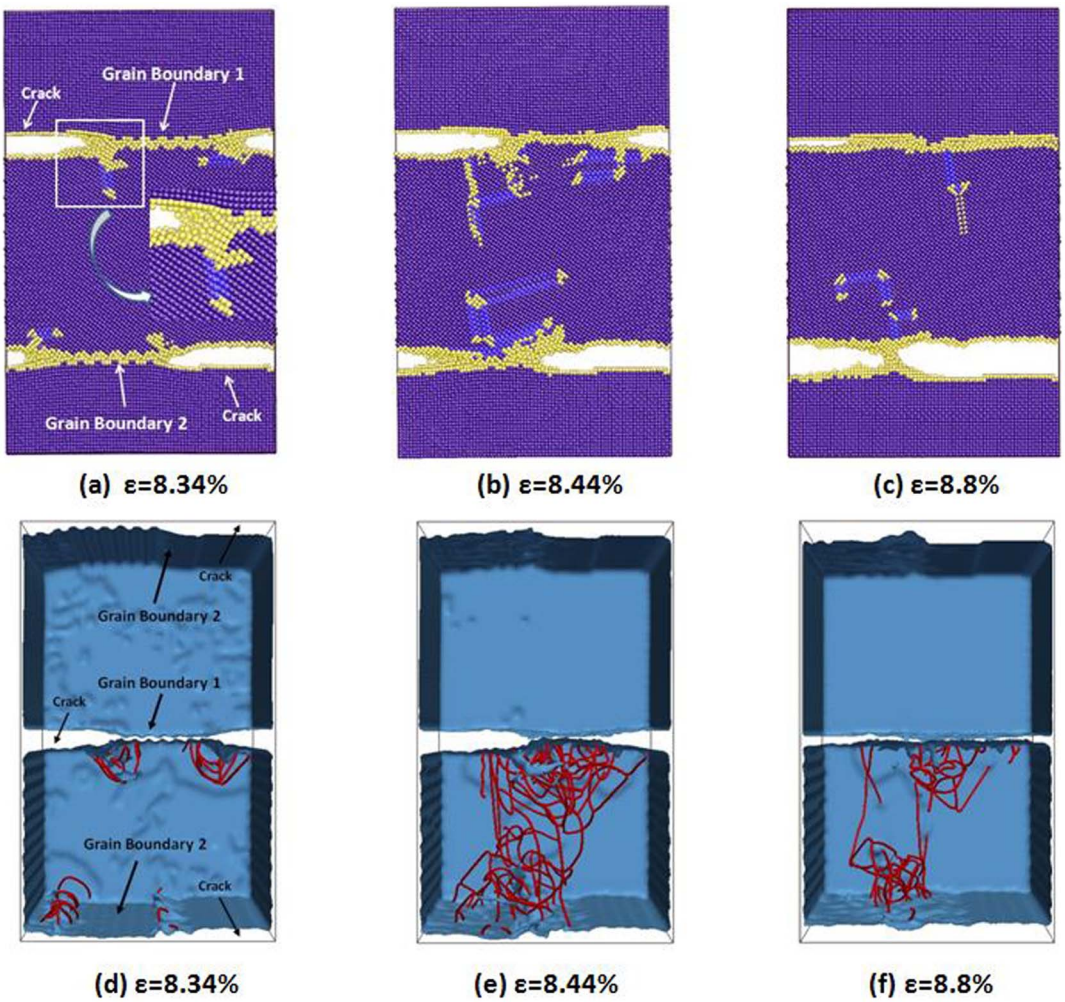

Figure 6 | Snapshots of Cu bicrystal with $\sum 5$ ($\phi = 18.43^{\circ}$) GB at different deformation stage under constrained tension boundary condition. Images (a)–(c) are colored according to the CNA parameter, atoms with perfect fcc structure are rendered as dark blue, atoms at GB area and the dislocation core are rendered as yellow, the light blue atoms indicate the stacking fault. Dislocation segments are extracted in (d)–(f).

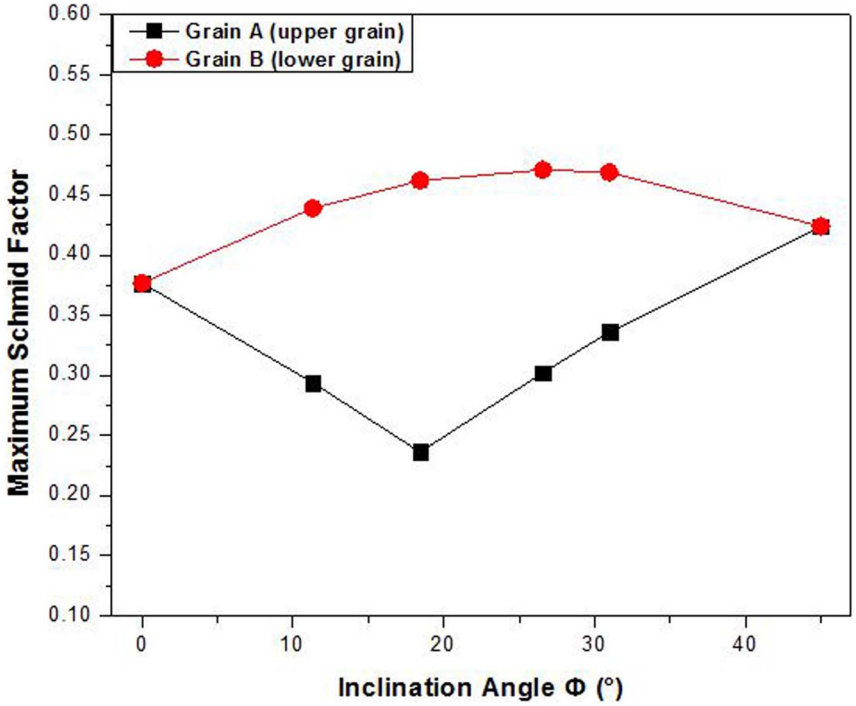

Figure 7 | The maximum Schmid factor as a function of GB inclination angle for grain A and grain B of the bicrystal models. Grain A and Grain B are defined in the bicrystal model in Fig. 9.

boundaries to dissociate into symmetric ones. The faceted boundary may do not even belong to any particular CSL. It was reported that the asymmetric $\sum$11 [1 1 0] GBs dissociated into a low-angle GB formed by Shockley partial dislocations and a high-angle non-$\sum$11 boundary. This kind of faceting into non-symmetric boundary structures and incorporating facets of non-$\sum$ boundary are not found in our simulation of $\sum$5 GBs, primarily because of the differences in boundary energy. Gokon et al.[42,43] experimentally determined the boundary energies of $\sum$11 [1 1 0] and $\sum$9 [1 1 0] tilt GBs in Cu for various inclination angles and, found the facet planes often correspond to a nearby symmetric or asymmetric boundary with low energy. According to the simulation result of $\sum$5 GB energy in our work, as seen in Fig. 2, the energy of asymmetric GBs is comparable with the $\phi = 45^\circ$ symmetric boundary and higher than the $\phi = 0^\circ$ symmetric boundary. From the point of view of energy, this may explain why such faceting of $\sum$5 asymmetric GBs occurs intend to the symmetric $\phi = 0^\circ$ and $\phi = 45^\circ$ planes.

Simulations reveal that dislocations are nucleated and emitted into both grains of the symmetric GBs once the maximum tensile stress has been reached, while this emission occurs only at the lower grain region in the asymmetric GBs at the beginning, and then the slip systems in the upper grain can be activated, as shown in S-Fig. 2. This phenomenon is expected for asymmetric GBs with inclination angles. Specifically, grains on each side of an asymmetric GB are oriented differently relative to the tensile stress direction, resulting in different Schmid factors. Therefore, the slip systems can be activated easily in the grain which associates with the higher Schmid factor, since the slip systems in this grain have higher resolved shear stress. Fig. 7 shows the maximum Schmid factor for both grains of the bicrystal models as a function of the inclination angle, from which we can see that the maximum Schmid factor is higher in the lower grain in all of the four cases of asymmetric GBs. This may explain why the partial dislocations preferentially nucleate first into the lower grain. For the asymmetric GBs, the nucleation of dislocations in the upper grain only occurs at higher strains when excessive dislocation emission severely alters the initial orientation of the lower grain.

In this study, we found that stress state can play an important role in the deformation mechanisms of nanocrystalline materials. Specifically, massive dislocation nucleation and propagation is the dominant mechanism during the tensile deformation under free tension boundary condition, as shown in S-Fig. 2. However, due to the transverse stress that applied perpendicular to the tensile stress under constrained tension boundary condition, the nucleation of dislocation and its propagation has been restrained. Meanwhile cracks are prone to initiate and can extend rapidly along the GB plane, which becomes the dominant mechanism during tension and leads to a more brittle mode of failure, as shown in S-Fig. 3. Moreover, only partial dislocation loops are nucleated from the Cu bicrystal interfaces during the tensile process under free tension boundary condition. However, it is interesting to find that full dislocation loops can also nucleate from boundary plane under the constrained tension boundary condition, as shown in Fig. 8 for the case of $\sum$5 ($\phi = 0^\circ$) GB. I Fig. 8(a), the leading partial dislocations have nucleated and moved away from the boundary plane, leaving behind an intrinsic stacking fault. As deformation proceeds, the trailing partial dislocation is evidenced to emit, resulting in a full dislocation loop and then pass through the periodic boundaries, as shown in Fig. 8(b) and (c). In previous reports[44–46], the trailing partial dislocation is considered can mainly nucleate from the fcc metals with high stacking fault energy (*e.g.* Al 146 mJ/m^2[47]), while the nucleation of full dislocation in the fcc metals with low stacking fault energy (*e.g.* Cu 44.4 mJ/m^2[48]) is thought to be difficult. To our understanding, few of the previous simulation studies has reported the full dislocations nucleation from Cu sample. Result of this study that full dislocations can be nucleated and propagate in Cu bicrystals under constrained tension boundary condition in return emphasizes the important role of stress state in the deformation mechanisms of nanocrystalline materials.

Methods

Model construction. In this study, bicrystal model with fixed orientation of the GB plane ($\theta = 36.9^\circ$ for $\sum$5 GBs) and fixed tilt axis ([0 0 1] axis) is employed, which enables a more controlled investigation of specific GB properties. Fig. 9 shows a

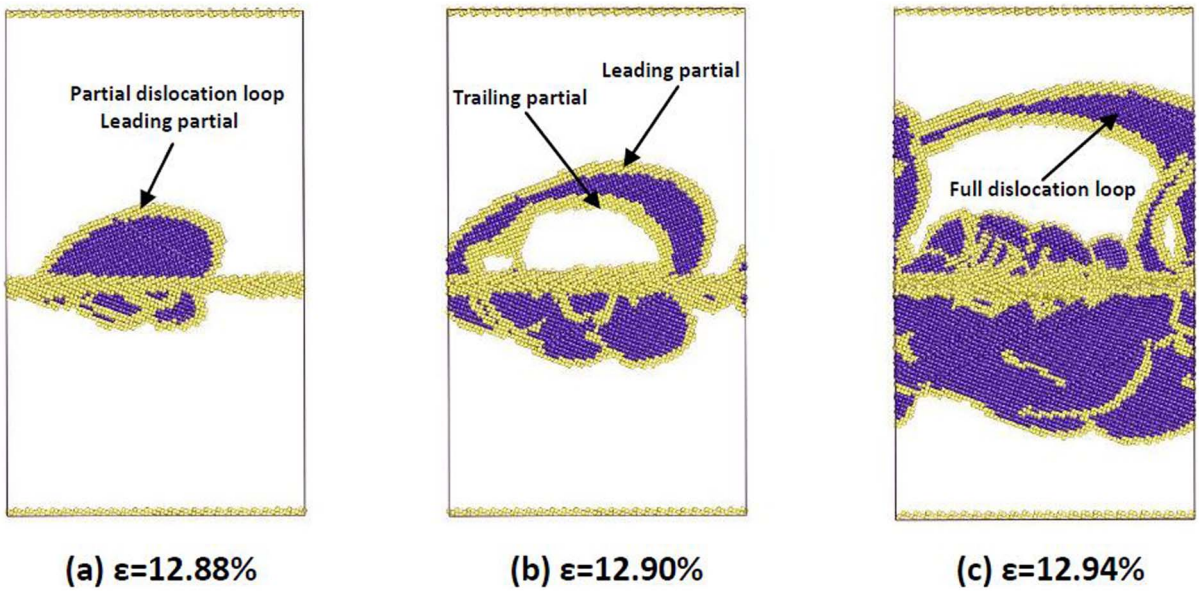

Figure 8 | Snapshots of Cu bicrystal with $\sum 5$ ($\phi = 0^\circ$) GB at different deformation stage under constrained tension boundary condition. Images are colored according to the CNA parameter. Atoms with perfect fcc structures are removed to facilitate viewing of the defective structures. Atoms colored with yellow organize the GB plane and the dislocation core, while the blue atoms represent the stacking fault.

schematic of the computational cell used in our simulations. A bicrystal model is created by constructing two separate crystal lattices (grain A and grain B in Fig. 9) with different crystallographic orientation and joining them together along the Y axis. The misorientation is defined as angle θ between the [1 0 0] direction of the two single crystal grains, and the inclination is defined as angle ϕ between the bisector of the misorientation and the boundary plane. The values of ϕ considered in this study and the Miller indices of the boundary plane are presented in S-Table 1. Due to the fourfold symmetry of the fcc lattice, the inclination angles from 0° to 45° cover all distinct boundary structures.

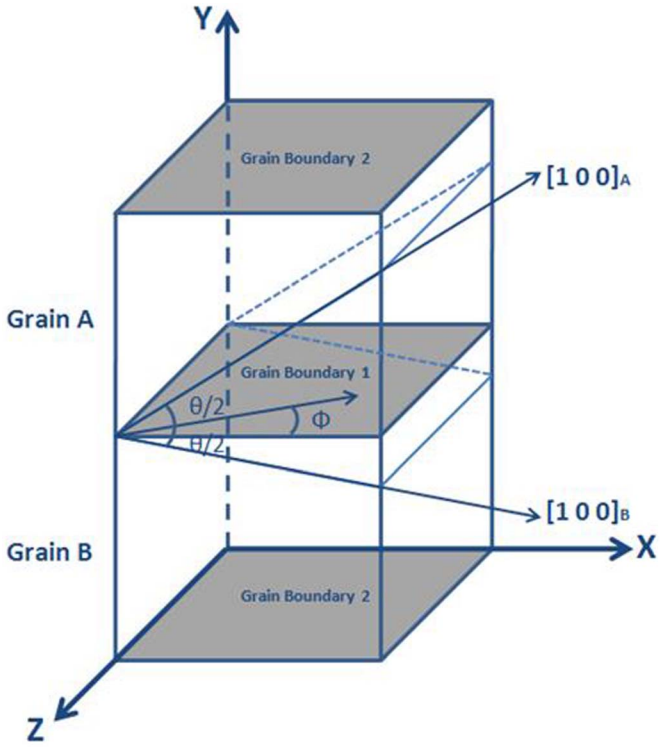

Figure 9 | Schematic of Cu bicrystal with a $\sum 5$ [0 0 1] asymmetric tilt grain boundary. The misorientation is defined as angle θ between the [1 0 0] direction of the two single crystal grains and the inclination is defined as angle ϕ between the boundary plane and the bisector of misorientation θ.

Periodic boundary conditions are used in all directions (X, Y and Z). Specifically, periodic boundary condition are applied to X and Z directions to simulate an infinite boundary plane between the two grains which can eliminate the effect of free surface. The periodic boundary condition in Y direction introduces a second boundary plane into the model. For each initial configuration, it is important to adjust the model size to construct identical atomic structures of the two boundary planes to ensure they have the same equilibrium structures and energies after energy minimization. Otherwise, the different equilibrium structures of the two boundary planes will result in, for example, a higher energy metastable plane at grain boundary 1 and a stable plane at grain boundary 2, which can significantly affect further simulation results. A number of initial "starting positions" of grain A and grain B are tested to find the possible GB structures[35,49,50]. Molecular statics calculations which employ a nonlinear conjugate gradient algorithm are conducted on all the tested GB structures to determine their minimum energy configurations.

GB energy calculation. After the procedure of energy minimization, the energy of each equilibrium GB structure is then calculated and compared to find the possible global minimum energy configuration. In this study, The GB structure with the lowest energy is regarded as the stable structure, while other GB structures with higher GB energy are reckoned to be metastable which will not be considered in our study. Since the periodic boundary condition in Y direction generates a pair of boundary planes in the bicrystal model, the energy associated with the grain boundary is calculated by the following equation:

$$\gamma_{GB} = \frac{E_{system} - N \cdot E_{atom}}{2A} \quad (4)$$

where E_{system} is the system energy of the equilibrium bicrystal model, E_{atom} is the potential energy of a single atom in the perfect Cu lattice (−3.54 eV), N is the total number of atoms contained in the model and A is the area of the GB plane.

Molecular dynamics simulation. All the simulations in this study are performed with the parallel molecular dynamics code LAMMPS[51]. The embedded-atom method (EAM) potential developed by Mishin et al. for copper[48] is employed, which can fit a large set of experimental and first-principles data. After the minimum energy configuration is attained, the simulation model is equilibrated using MD in the isobaric-isothermal (NPT) ensemble at a pressure of 0 bar and a temperature of 10 K for 20 ps. A constant rate of 2×10^8 s^{-1} is applied perpendicular to the boundary plane (along Y direction) at a temperature of 10 K. Tensile deformation is performed under either 'free' or 'constrained' boundary condition. These boundary conditions are very similar to those used by Kitamura et al.[52] and Spearot et al.[53] to study the effect of boundary condition on tensile deformation of nickel single crystal and copper bicrystal respectively. Under free tension boundary condition, the boundaries in the lateral directions are allowed to expand or contract during the deformation process and the transverse stresses are kept free ($\sigma_{xx} = \sigma_{zz} = 0$). Under constraint tension boundary condition, computational models are strained at a constant rate along the Y axis while keeping the model dimensions along the X and Z axis fixed ($\varepsilon_{xx} = \varepsilon_{zz} = 0$). This boundary condition considers the transverse stress along the X and Z axis during the tensile deformation process. The schematic of tension simulation is shown in S-Fig. 1. The visualization tools Atomeye[54] and Ovito[55] are used to illustrate of the

bicrystal models. The common neighbor analysis (CNA) technique[34] is used to identify the defect structure and its evolution during the simulations. The dislocation extraction algorithm (DXA)[37,38] is used to convert identified dislocations into continuous lines and compute their Burgers vectors.

1. Sutton, A. P. & Balluffi, R. W. *Interfaces in crystalline materials.* (Oxford, Clarendon, 1995).
2. Van Swygenhoven, H. & Derlet, P. M. Grain-boundary sliding in nanocrystalline fcc metals. *Phys. Rev. B* **64**, 224105 (2001).
3. Ma, E. Watching the Nanograins Roll. *Science* **305**, 623–624 (2004).
4. Shan, Z. *et al*. Grain Boundary-Mediated Plasticity in Nanocrystalline Nickel. *Science* **305**, 654–657 (2004).
5. Yamakov, V., Wolf, D., Phillpot, S. R. & Gleiter, H. Grain-boundary diffusion creep in nanocrystalline palladium by molecular-dynamics simulation. *Acta Mater.* **50**, 61–73 (2002).
6. Van Swygenhoven, H., Derlet, P. M. & Hasnaoui, A. Atomic mechanism for dislocation emission from nanosized grain boundaries. *Phys. Rev. B* **66**, 024101 (2002).
7. Kumar, K. S., Van Swygenhoven, H. & Suresh, S. Mechanical behavior of nanocrystalline metals and alloys. *Acta Mater.* **51**, 5743–5774 (2003).
8. Liao, X. Z. *et al*. Deformation mechanism in nanocrystalline Al: Partial dislocation slip. *Appl. Phys. Lett.* **83**, 632–634 (2003).
9. Budrovic, Z., Van Swygenhoven, H., Derlet, P. M., Van Petegem, S. & Schmitt, B. Plastic Deformation with Reversible Peak Broadening in Nanocrystalline Nickel. *Science* **304**, 273–276 (2004).
10. Van Swygenhoven, H., Derlet, P. M. & Frøseth, A. G. Nucleation and propagation of dislocations in nanocrystalline fcc metals. *Acta Mater.* **54**, 1975–1983 (2006).
11. Rohrer, G. S. *et al*. The distribution of internal interfaces in polycrystals. *Mater. Res. Adv. Tech.* **95**, 197–214 (2004).
12. Saylor, D. M., El Dasher, B. S., Rollett, A. D. & Rohrer, G. S. Distribution of grain boundaries in aluminum as a function of five macroscopic parameters. *Acta Mater.* **52**, 3649–3655 (2004).
13. Kim, C.-S., Rollett, A. D. & Rohrer, G. S. Grain boundary planes: New dimensions in the grain boundary character distribution. *Scr. Mater.* **54**, 1005–1009 (2006).
14. Minkwitz, C., Herzig, C., Rabkin, E. & Gust, W. The inclination dependence of gold tracer diffusion along a Σ3 twin grain boundary in copper. *Acta Mater.* **47**, 1231–1239 (1999).
15. Miyamoto, H., Ikeuchi, K. & Mimaki, T. The role of grain boundary plane orientation on intergranular corrosion of symmetric and asymmetric [1 1 0] tilt grain boundaries in directionally solidified pure copper. *Scr. Mater.* **50**, 1417–1421 (2004).
16. Gemming, T., Nufer, S., Kurtz, W. & Rühle, M. Structure and Chemistry of Symmetrical Tilt Grain Boundaries in α-Al2O3: I, Bicrystals with "Clean" Interface. *J. Am. Ceram. Soc.* **86**, 581–589 (2003).
17. Lee, S. B., Sigle, W., Kurtz, W. & Rühle, M. Temperature dependence of faceting in Σ5(310)[001] grain boundary of SrTiO3. *Acta Mater.* **51**, 975–981 (2003).
18. Lee, S. B., Sigle, W. & Rühle, M. Faceting behavior of an asymmetric SrTiO3 Σ5 [001] tilt grain boundary close to its defaceting transition. *Acta Mater.* **51**, 4583–4588 (2003).
19. Lee, S. B. & Kim, Y.-M. Kinetic roughening of a Σ5 tilt grain boundary in SrTiO3. *Acta Mater.* **57**, 5264–5269 (2009).
20. Bourret, A., Rouviere, J. L. & Penisson, J. M. Structure Determination of Planar Defects in Crystals of Germanium and Molybdenum by HREM. *Acta Crystallogr. A* **44**, 838–847 (1988).
21. Lee, H. S., Mizoguchi, T., Yamamoto, T., Kang, S. J. L. & Ikuhara, Y. Characterization and atomic modeling of an asymmetric grain boundary. *Phys. Rev. B* **84**, 195319 (2011).
22. Lin, E. Q., Shi, H. J., Niu, L. S. & Jin, E. Z. Shock response of copper bicrystals with a Σ3 asymmetric tilt grain boundary. *Comput. Mater. Sci.* **59**, 94 (2012).
23. Sheng-Nian, L., Germann, T. C., Tonks, D. L. & Qi, A. Shock wave loading and spallation of copper bicrystals with asymmetric Σ3 [110] tilt grain boundaries. *J. Appl. Phys.* **108**, 093526 (2010).
24. Zhang, H., Duy, D. & Srolovitz, D. J. Effects of boundary inclination and boundary type on shear-driven grain boundary migration. *Philos. Mag.* **88**, 243–256 (2008).
25. Zhang, H., Mendelev, M. I. & Srolovitz, D. J. Mobility of Σ5 tilt grain boundaries: Inclination dependence. *Scr. Mater.* **52**, 1193–1198 (2005).
26. Tschopp, M. A. & McDowell, D. L. Structures and energies of Σ3 asymmetric tilt grain boundaries in copper and aluminium. *Philos. Mag.* **87**, 3147–3173 (2007).
27. Tschopp, M. A. & McDowell, D. L. Dislocation nucleation in Σ3 asymmetric tilt grain boundaries. *Int. J. Plasticity* **24**, 191–217 (2008).
28. Saylor, D. M., Morawiec, A. & Rohrer, G. S. Distribution of grain boundaries in magnesia as a function of five macroscopic parameters. *Acta Mater.* **51**, 3663–3674 (2003).
29. Rohrer, G. S., Randle, V., Kim, C. S. & Hu, Y. Changes in the five-parameter grain boundary character distribution in α-brass brought about by iterative thermomechanical processing. *Acta Mater.* **54**, 4489–4502 (2006).
30. Liu, L., Wang, J., Gong, S. K. & Mao, S. X. Atomistic observation of a crack tip approaching coherent twin boundaries. *Sci. Rep.* **4** (2014).
31. Tschopp, M. A. & McDowell, D. L. Asymmetric tilt grain boundary structure and energy in copper and aluminium. *Philos. Mag.* **87**, 3871–3892 (2007).
32. Mendelev, M. I., Zhang, H. & Srolovitz, D. J. Grain boundary self-diffusion in Ni: Effect of boundary inclination. *J. Mater. Res.* **20**, 1146–1153 (2005).
33. Zhang, H., Srolovitz, D. J., Douglas, J. F. & Warren, J. A. Characterization of atomic motion governing grain boundary migration. *Phys. Rev. B* **74**, 115404 (2006).
34. Schiøtz, J., Di Tolla, F. D. & Jacobsen, K. W. Softening of nanocrystalline metals at very small grain sizes. *Nature* **391**, 561–563 (1998).
35. Rittner, [1 1 0] symmetric tilt grain-boundary structures in fcc metals with low stacking-fault energies. *Phys. Rev. B* **54**, 6999–7015 (1996).
36. Spearot, D. E., Jacob, K. I. & McDowell, D. L. Dislocation nucleation from bicrystal interfaces with dissociated structure. *Int. J. Plasticity* **23**, 143–160 (2007).
37. Stukowski, A. & Albe, K. Extracting dislocations and non-dislocation crystal defects from atomistic simulation data. *Model. Simul. Mater. Sci. Eng.* **18**, 085001 (2010).
38. Stukowski, A. Structure identification methods for atomistic simulations of crystalline materials. *Model. Simul. Mater. Sci. Eng.* **20**, 045021 (2012).
39. Spearot, D. E., Tschopp, M. A., Jacob, K. I. & McDowell, D. L. Tensile strength of <1 0 0> and <1 1 0> tilt bicrystal copper interfaces. *Acta Mater.* **55**, 705–714 (2007).
40. Sutton, A. P. & Balluffi, R. W. On geometric criteria for low interfacial energy. *Acta Mater.* **35**, 2177–2201 (1987).
41. Brown, J. A. & Mishin, Y. Dissociation and faceting of asymmetrical tilt grain boundaries: Molecular dynamics simulations of copper. *Phys. Rev. B* **76**, 134118 (2007).
42. Goukon, N., Yamada, T. & Kajihara, M. Boundary energies of Σ11 [1 1 0] asymmetric tilt boundaries in Cu determined from the shape of boundary silica particles. *Acta Mater.* **48**, 2837–2842 (2000).
43. Gokon, N. & Kajihara, M. Experimental determination of boundary energies of Σ9 [1 1 0] asymmetric tilt boundaries in Cu. *Mater. Sci. Eng. A* **477**, 121–128 (2008).
44. Van Swygenhoven, H., Derlet, P. M. & Frøseth, A. G. Stacking fault energies and slip in nanocrystalline metals. *Nature mater.* **3**, 399–403 (2004).
45. Yamakov, V., Wolf, D., Phillpot, S. R., Mukherjee, A. K. & Gleiter, H. Deformation-mechanism map for nanocrystalline metals by molecular-dynamics simulation. *Nature mater.* **3**, 43–47 (2004).
46. Spearot, D. E., Jacob, K. I. & McDowell, D. L. Nucleation of dislocations from [0 0 1] bicrystal interfaces in aluminum. *Acta Mater.* **53**, 3579–3589 (2005).
47. Mishin, Y., Mehl, M. J., Papaconstantopoulos, D. A., Voter, A. F. & Kress, J. D. Structural stability and lattice defects in copper: Ab initio, tight-binding, and embedded-atom calculations. *Phys. Rev. B* **63**, 2241061–22410616 (2001).
48. Mishin, Y., Farkas, D., Mehl, M. J. & Papaconstantopoulos, D. A. Interatomic potentials for monoatomic metals from experimental data and ab initio calculations. *Phys. Rev. B* **59**, 3393–3407 (1999).
49. Olmsted, D. L., Foiles, S. M. & Holm, E. A. Survey of computed grain boundary properties in face-centered cubic metals: I. Grain boundary energy. *Acta Mater.* **57**, 3694–3703 (2009).
50. Zhang, L., Lu, C., Michal, G., Tieu, K. & Cheng, K. Molecular dynamics study on the atomic mechanisms of coupling motion of [0 0 1] symmetric tilt grain boundaries in copper bicrystal. *Mater. Res. Express* **1**, 015019 (2014).
51. Plimpton, S. Fast Parallel Algorithms for Short-Range Molecular Dynamics. *J. Comput. Phys.* **117**, 1–19 (1995).
52. Kitamura, T., Yashiro, K. & Ohtani, R. Atomic simulation on deformation and fracture of nano-single crystal of nickel in tension. *JSME Int. J. A* **40**, 430–435 (1997).
53. Spearot, D. E. Evolution of the E structural unit during uniaxial and constrained tensile deformation. *Mech. Res. Commun.* **35**, 81–88 (2008).
54. Li, J. AtomEye: an efficient atomistic configuration viewer. *Model. Simul. Mater. Sci. Eng.* **11**, 173–177 (2003).
55. Stukowski, A. Visualization and analysis of atomistic simulation data with OVITO–the Open Visualization Tool. *Model. Simul. Mater. Sci. Eng.* **18**, 015017 (2010).

Acknowledgments

This work was supported by an Australia Research Council Discovery Grant (DP0773329). Simulations were performed using the HPC cluster of University of Wollongong and the computing facilities provided by NCI National Facility of Australia. Dr. Alexander Stukowski from Darmstadt University of Technology is greatly appreciated for sharing the DXA code. The authors gratefully acknowledge the help of Dr. Madeleine Strong Cincotta in the final language editing of this paper. Z.L. would like to acknowledge the financial support from China Scholarship Council (CSC).

Author contributions

L.Z. constructed the simulation models and conducted the MD simulations. L.Z. and C.L. prepared the manuscript. K.T. made the plan and conduct the technical reviews. All the authors discussed the results and contributed to revising the paper.

Additional information

Supplementary information accompanies this paper at http://www.nature.com/scientificreports

Competing financial interests: The authors declare no competing financial interests.

How to cite this article: Zhang, L., Lu, C. & Tieu, K. Atomistic Simulation of Tensile Deformation Behavior of ∑5 Tilt Grain Boundaries in Copper Bicrystal. *Sci. Rep.* **4**, 5919; DOI:10.1038/srep05919 (2014).